





First determination of whistler wave dispersion relation in superhot ($T_e > 5$ keV) plasmasW. Z. Zhang , H. S. Fu *, J. B. Cao, Z. Wang , W. D. Fu, Y. Y. Liu , and Y. Yu*School of Space and Environment, Beihang University, Beijing, China
and Key Laboratory of Space Environment Monitoring and Information Processing,
Ministry of Industry and Information Technology, Beijing, China*

(Received 30 August 2023; accepted 21 December 2023; published 1 March 2024)

A whistler wave is a fundamental electromagnetic radiation. In the universe, it transmits information through diverse mediums at audio frequencies. To know the properties of such a radio, one should determine how its frequency (energy) changes with its wavelength (momentum). The relation between them is called the dispersion relation, which encodes essential information on the kinetics. Although the dispersion relation governs the majority of the whistler properties, the experimental determination of their entire dispersion is still a challenge today. Especially in high-temperature mediums, the group velocity dispersion properties of whistlers are still unverified by spacecraft experiments despite their practical importance. Here, for the first time, we experimentally determine the dispersion relation of whistler waves in superhot ($T_e > 5$ keV) plasmas by the magnetospheric multiscale mission located in a magnetotail plasma sheet. Our result unmasks the characteristics of whistler waves at elevated temperatures and exhibits the evolution of their group velocity dispersion from positive to negative, which agrees well with kinetic theory, opening the door to controlled radio excitation and transport.

DOI: [10.1103/PhysRevResearch.6.L012047](https://doi.org/10.1103/PhysRevResearch.6.L012047)**I. INTRODUCTION**

Whistler waves, also known as whistlers, are right-hand polarized electromagnetic (radio) waves propagating at frequencies ranging from low-hybrid frequency f_{lh} to electron-cyclotron frequency f_{ce} [1,2]. The name “whistlers” dates back 130 years to unexplained whistling sounds heard on long telephone lines [3], and Barkhausen *et al.* first clearly described this type of radio wave in 1919 by using ground-based radio receivers [4]. Whistlers are possibly one of the first-observed and best-known plasma wave phenomena, which exist widely throughout the whole universe, including the ocean [5], atmosphere [6], radiation belts [7], planetary magnetospheres [8–12], stellar corona [13], solar wind [14], galaxy clusters [15], and interstellar medium [16]; also, they can exist in laboratory experiments [17,18]. There are various mechanisms that can lead to the emission of waves propagating in the whistler branch, such as lightning strikes and anisotropic electron distributions [19–22].

Although whistler waves have been studied for over 100 years, many interesting questions remain unsolved. Satellite and ground-based measurements have shown that the whistler waves can be converted into audio and transmit radio signals [1], whose melody sounds different in different mediums, such as lightning-generated whistlers, plasmaspheric hiss, lion

roars, and choruses [23]. However, the intrinsic properties of whistler waves controlled by their dispersion relation [24], such as phase velocities, group velocities, wave vectors, and energy distribution in three-dimensional wave-vector space, remain enigmas in spacecraft experiments. On the other hand, cold plasma theory assumes that whistler waves have dispersive properties (group and phase velocities are frequency-dependent) [24,25], which are formed by nonlinear processes [26], characterized by frequency chirping—rising or falling tones in the time-frequency spectrogram [27]—and highly contribute to optical communication systems and magnetic reconnection (a crucial plasma process during which magnetic topology changes and magnetic energy is converted to particle energy) [28]. However, such a fundamental property is stuck in theory [26,29–32] and is still unverified in spacecraft experiments despite their application value in high-temperature mediums.

To thoroughly unveil the propagation dynamics of whistler waves, especially to understand how they are involved in wave-particle interactions [27,33–36] (such as particle heating, acceleration, scattering, and absorption) during high-temperature physical processes [37–39] (e.g., magnetic reconnection and thermonuclear fusion), determining their dispersion relations should be the first step. With advanced multi-spacecraft missions and innovative methods, it is now possible to independently measure frequencies and wave vectors, transform them into a plasma frame, and experimentally resolve the dispersion relation. Besides, among the entire universe environment, within reach of satellites, the electron temperature at the Earth’s magnetotail may be one of the highest, which can reach up to 10 keV (100 million Kelvin) [40,41], dozens to hundreds of times higher than previous studies on whistlers [42–45]. Compared to characteristic

*Corresponding author: huishanf@gmail.com

Published by the American Physical Society under the terms of the [Creative Commons Attribution 4.0 International](https://creativecommons.org/licenses/by/4.0/) license. Further distribution of this work must maintain attribution to the author(s) and the published article’s title, journal citation, and DOI.

temperatures in laboratory, space, and astrophysical plasmas ([46–50], see Fig. 1(a)), Earth’s magnetotail provides an ideal laboratory for studying whistler waves in high-temperature plasmas [51,52]. Being satisfied with these criteria, in this Letter we aim to provide the first experimental determination of the dispersion relation for whistler waves in superhot plasmas ($T_e > 5$ keV). We utilize data from the magnetospheric multiscale (MMS) mission [53] and employ the dispersion relation from timing (DRAFT) technique [54]. Specifically, the instruments used are fast plasma investigation [55] and the flux gate magnetometer [56]; the applied technique DRAFT is designed for analyzing space plasma waves, allowing us to derive dispersion relations and the three-dimensional \mathbf{K} -spectrum of plasma waves [54].

II. EXPERIMENT OVERVIEW

The event of interest (low-frequency whistler waves in superhot plasmas) was found in the Earth’s magnetotail [see the red star in the sketch in Fig. 1(b)]. Specifically, the fluctuation was detected by MMS on 19 June 2017 at about 03:57:46 UT, when the four MMS spacecraft were located at $[-16.8, -0.3, 1.6] R_E$ in GSM coordinates with average separations of ~ 37 km. Figures 1(c)–1(h) show an overview of this event. Before 03:57:37.5 UT, MMS observed a weak magnetic field [$B_x < 2$ nT, Fig. 1(c)], a high plasma density [$N_e > 0.35$ cm $^{-3}$, Fig. 1(d)], and a low electron temperature [$T_e \approx 1.5$ keV, Fig. 1(e)], indicating that MMS was located at the magnetotail neutral sheet. Around 07:57:37.5 UT, MMS detected a sudden increase of magnetic field from $B_z \approx 5$ nT to $B_z \approx 17$ nT [Fig. 1(c)], a significant drop in plasma density from $N_e \approx 0.4$ cm $^{-3}$ to $N_e \approx 0.05$ cm $^{-3}$ [Fig. 1(d)], a dramatic increase in electron temperature from $T_e \approx 1.5$ keV to $T_e \approx 5$ keV [Fig. 1(e)], and a fast ion flow with a local speed approaching 400 km/s [Fig. 1(f)]. Such an abrupt change from 07:57:37.5 to 07:57:39 UT can be identified as a reconnection front (RF, also called a dipolarization front), which is consistent with typical characteristics of the RFs observed in the plasma sheet [57–61]. RFs are sharp magnetic boundaries separating hot-tenuous plasmas (possibly from the reconnection site) from cold-dense plasmas in the terrestrial magnetotail. Behind the RF, the ions and electrons get heated and accelerated inside the traveling high B_z region from 03:57:40 to 03:57:50 UT, associated with sharp changes in the particle energy spectrum [Figs. 1(g) and 1(h)]. Such changes behind RFs can be identified as the dipolarizing flux bundle (DFB), a scenario widely reported in previous studies [57,61–63]. DFB and RF have both been suggested to be parts of the reconnection outflow. Specifically, RF is the sharp boundary leading DFB, and DFB is the associated structure of DF.

Inside the dipolarizing flux bundle, interestingly, where B_z is typically expected to stay steadily strong, MMS observed a localized magnetic field depletion structure [see the gray shade in Figs. 1(c)–1(f)], characterized by a dramatic decrease of the total magnetic field from $B_t \approx 10$ nT to $B_t \approx 5$ nT [Fig. 1(c)] and an increase in plasma density from $N_e \approx 0.1$ cm $^{-3}$ to $N_e \approx 0.16$ cm $^{-3}$ [Fig. 1(d)], based on which we interpret such structure as a magnetic hole (MH) [64,65]. The magnetic hole is embedded inside a fast ion flow with a maximum speed approaching 900 km/s [Fig. 1(f)], which is

faster than the local ion flow at the RF. The superhot electrons [$T_e \approx 5$ –6 keV, see Fig. 1(e)] in the magnetic hole exhibit an apparent electron temperature anisotropy, with the perpendicular electron temperature relatively higher than the parallel one, which has been suggested to be a consequence of betatron heating. Interestingly, one can see that the magnetic hole hosts strong low-frequency fluctuations of magnetic fields in such high-temperature ($T_e > 5$ keV) plasmas.

III. DETERMINATION OF THE DISPERSION RELATION

Figure 2 presents detailed magnetic signals of the periodic magnetic fluctuations, which are indications of plasma waves. It is noticed that such waves were observed at the interior of the magnetic hole during 03:57:44.5–03:57:46 UT. As can be seen, four MMS satellites measured quite similar wavefronts, applicable for multi-spacecraft wave analyses. We employ the DRAFT method to determine the nature of this wave [54]. Such a method, calculating the phase velocity of a single-frequency wave by using the timing analysis, dividing the wave frequency by the phase velocity to obtain the wave vector, and solving the dispersion relation (ω - k relation) by considering all frequency channels, provides comprehensive analyses of waves [including the spectrum of wave power, wave normal angle, wave vector, wave phase velocity, and the three-dimensional (3D) \mathbf{K} -spectrum]. We have quantitatively defined three error parameters—namely the match of amplitude (MOA), the ratio of half-wavelength to spacecraft separation ($\lambda/2R_{sc}$), and the correlation coefficient (CC)—to judge the reliability of the DRAFT technique. These three criteria could be applied to the current study because they could guarantee that the four spacecraft detect the same wavefronts, and guarantee that the time shift is accurate enough. Generally speaking, the larger these parameters, the more accurate the results. Empirically, we set the threshold of the three parameters as “MOA > 0.5 , $\lambda/2R_{sc} > 1$, CC > 0.8 ” to guarantee that the results derived from the DRAFT method are accurate (see the validation by Zhang *et al.* [54]).

Figure 3 shows the results of wave propagation analyses. Concretely, we present the spectrum of the wave power, wave phase velocity, wave vector, and wave normal angle in Figs. 3(a)–3(d). Furthermore, we compare the results of wave normal angles obtained by DRAFT and the previously used SVD [66] method in Figs. 3(d) and 3(e). Finally, we provide the quantitative error parameters in Figs. 3(f)–3(h). As can be seen, there are strong wave emissions roughly between $0.1 f_{ce}$ (black lines) and $0.3 f_{ce}$ (red lines) during 03:57:45–03:57:45.7 UT [Fig. 3(a)]. These electromagnetic waves (the electric field fluctuation is not shown here) possess a phase-velocity magnitude around 9000 km s $^{-1}$ [Fig. 3(b)], a wave number near 0.02 km $^{-1}$ [Fig. 3(c)], and a wave normal angle smaller than 20° [Fig. 3(d)]. These properties should be derived accurately because the three parameters we defined are considerably large in the frequency range 0.1 – $0.3 f_{ce}$: $\lambda/2R_{sc} > 3$ [see Fig. 3(f)], CC > 0.8 [see Fig. 3(g)], MOA > 0.7 [see Fig. 3(h)]. Also, our results are well consistent with SVD results in solving wave normal angles [see Figs. 3(d) and 3(e)], validating the results of DRAFT. We can ignore the uniform Doppler-shift effect in this event: $\omega_{pls} = \omega_{sc} - \mathbf{V}_i \cdot \mathbf{k}$, which generally converts the wave frequency from the spacecraft

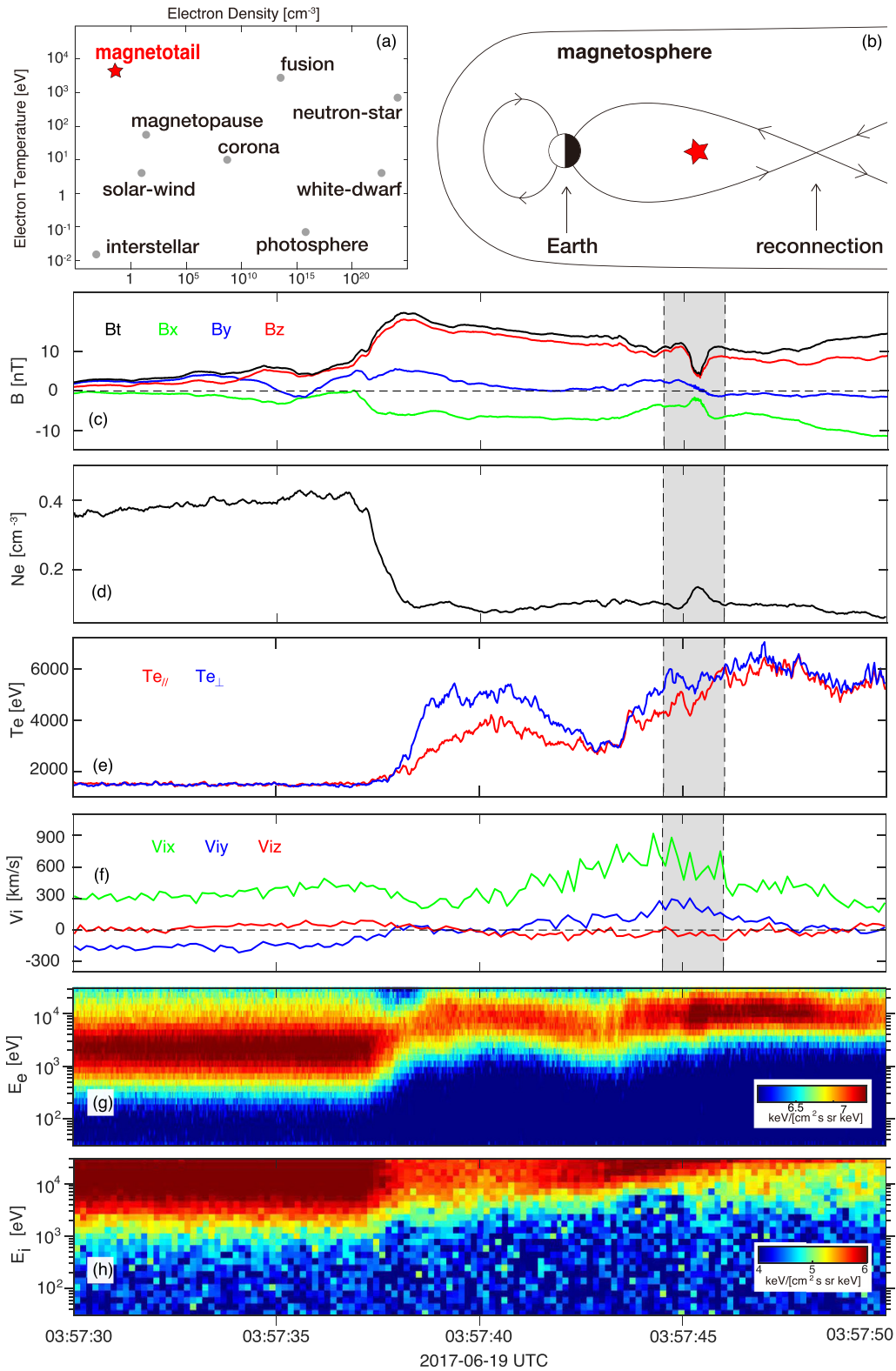


FIG. 1. Overview of the experiment. (a) Plasma temperature vs number density diagram. (b) Sketch of the Earth’s magnetosphere. (c)–(f) MMS1 observations of the Earth’s magnetotail plasma sheet on June 19, 2017. (c) Magnetic field. (d) Plasma density. (e) The electron temperature in parallel and perpendicular directions. (f) Ion bulk flow velocities. (g) The differential energy fluxes of electrons. (h) The differential energy fluxes of ions. The gray shade between the two black dotted lines highlights the low-frequency whistler waves inside a magnetic hole behind the reconnection front.

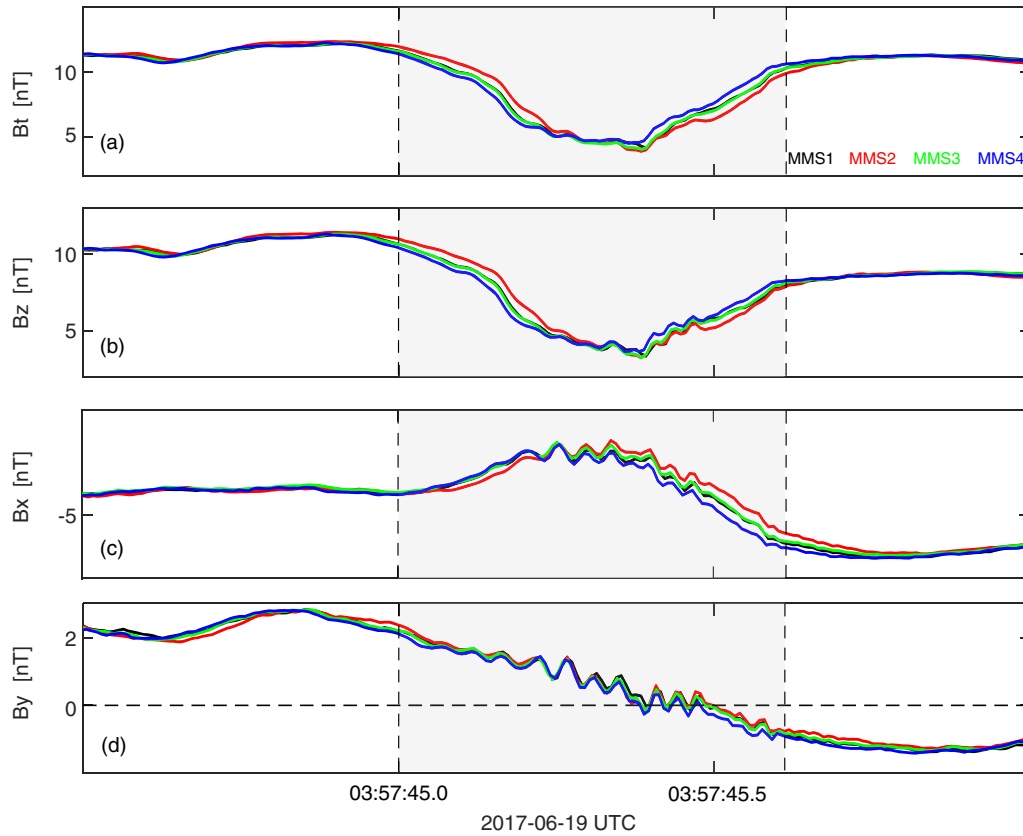


FIG. 2. Four MMS measurements of magnetic fields B_t , B_z , B_x , B_y . MMS1-MMS4 data are shown in black, red, green, and blue, respectively.

frame to the ion rest frame, because here the wave velocity (~ 9000 km/s) is much faster than the local ion velocity (~ 700 km/s), meaning that the wave frequencies can be regarded as in the plasma coordinate system. Combing these wave propagation properties (some results of SVD not shown here), these electromagnetic waves inside the magnetic hole have large positive ellipticities (~ 1), small propagation angles ($\theta < 20^\circ$) with respect to the ambient magnetic field, large planarization (~ 1), as well as fast wave phase-velocity (~ 9000 km/s). Therefore, these waves should correspond to right-handed polarized and paralleling-propagating whistlers. In fact, this wave has been identified as electron-scale whistlers coupled with sub-ion-scale magnetic field dissipation [67].

Figures 4(a) and 4(b) display a scatter plot of determined frequencies and wave numbers reorganized from the data in Figs. 3(a)–3(d), with the colored data points denoting the wave power [Fig. 4(a)] and the wave phase speed [Fig. 4(b)], respectively. Such reorganizations of data in the plasma coordinate system constitute the experimental dispersion relation of targeted waves at the frequency range 10–100 Hz during 03:57:45–03:57:45.7 UT. In particular, to guarantee that the results belong to wave activities, we only consider those sampling counts above limited wave power ($> 8 \times 10^{-5}$ nT²/Hz); to guarantee that the results are accurate enough, we have removed sampling counts with small MOA ($\text{MOA} < 0.5$), small $\lambda/2R_{sc}$ ($\lambda/2R_{sc} < 1$), and small CC ($\text{CC} < 0.8$) [Figs. 3(f)–3(h)]. It should also be mentioned that we only consider waves having propagation angles $0 < \theta < 30^\circ$ [Fig. 3(d)],

because considering the above criteria, sampling counts with $60^\circ < \theta < 90^\circ$ are in small quantity and neglectable. Frequencies and wave numbers are normalized to local plasma scales: the electron gyrofrequency ω_{ce} and electron gyroradius ρ_e . Apparently, the scatter points [Fig. 4(a)] directly reveal that these waves at frequencies around $0.1 - 0.3\omega_{ce}$ are dispersive: wave speed changes with frequency. Also, the scatter points [Fig. 4(b)] indicate that the wave phase velocity becomes faster when the frequency rises and the wave number decreases, which is intelligible. When such waves with different frequency components are superimposed, we are more concerned about their group velocity, which describes the velocity at which energy and information in a pulse or signal travel.

To investigate the group velocity dispersion and identify the wave mode exactly, experimental data were compared to the numerical solution computed using a kinetic dispersion relation solver: Waves in Homogeneous Anisotropic Multicomponent Plasmas (WHAMP) [68]. Here, we set $N_e = 0.15 \text{ cm}^{-3}$, $B_0 = 5 \text{ nT}$, $T_e = 5500 \text{ eV}$, and temperature anisotropy $T_{e\perp}/T_{e\parallel} = 1.2$ to match the superhot local plasma conditions in association with the observed wave inside the magnetic hole. Within this model, the only wave mode predicted to propagate at the observed frequencies is the whistler wave. The numerical solution of dispersion relations under the above conditions is drawn by black solid lines in Figs. 4(a) and 4(b). Clearly, the theory solution from WHAMP exhibits the evolution of group velocity dispersion from $\partial^2 k / \partial^2 \omega > 0$ at $\sim 0.1\omega_{ce}$ to $\partial^2 k / \partial^2 \omega < 0$ at $0.2\omega_{ce}$, indicating a nonlinear

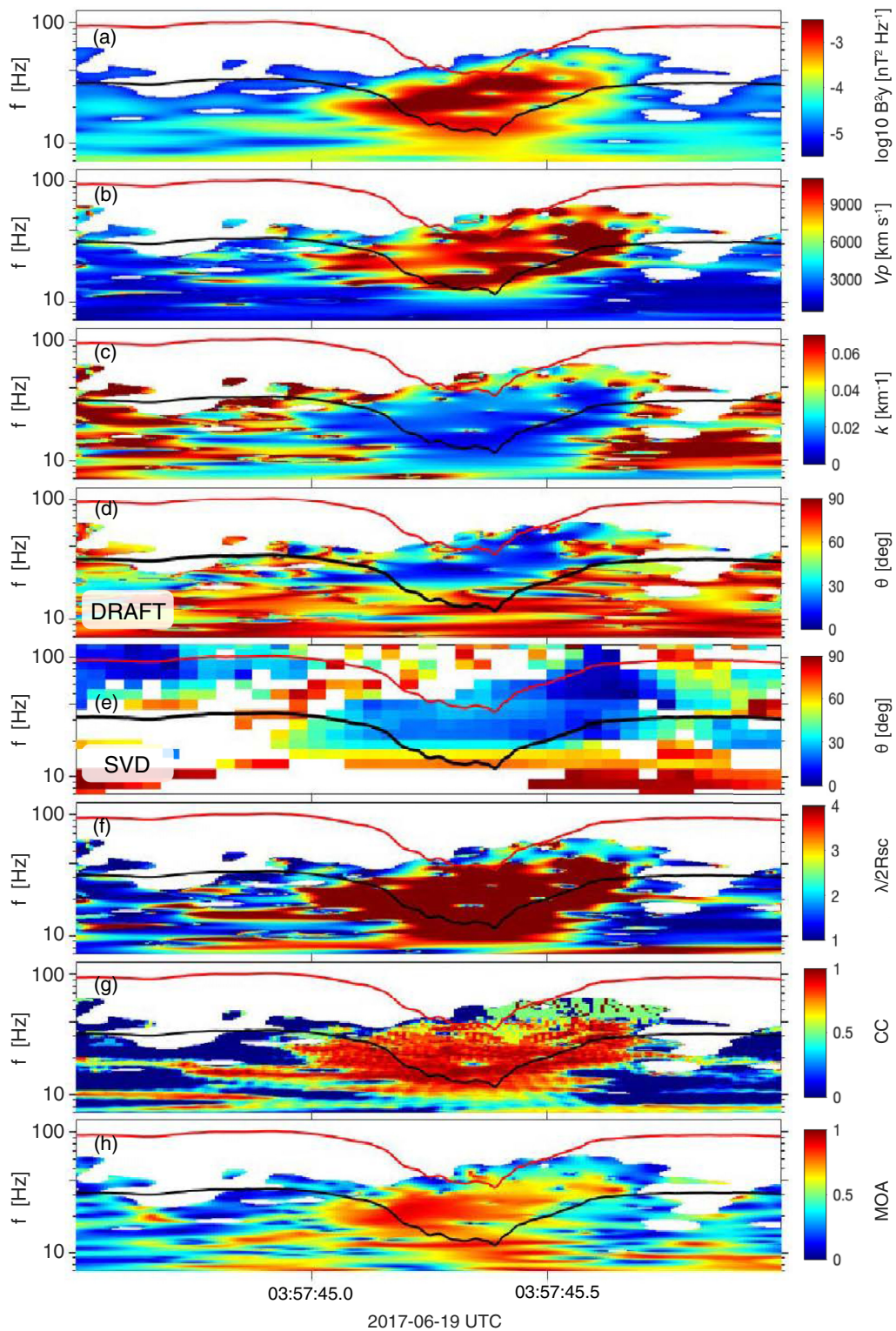


FIG. 3. Propagation dynamics of the whistler wave. (a) The average wave power density of the magnetic field from four spacecraft. (b) The wave phase velocity. (c) The wave vector. (d),(e) The wave normal angle by the DRAFT and the SVD method, respectively. (f)–(h) Error parameters. (f) The ratio of half-wavelength to spacecraft separation ($\lambda/2R_{sc}$). (g) CC. (h) MOA. Here the obtained phase velocity and wave vector are essentially three-dimensional vectors (\mathbf{v} , \mathbf{k}), but for simplicity we only show their modulus, i.e., the phase-velocity magnitude ($v_p = |\mathbf{v}|$) and the wave number ($k = |\mathbf{k}|$). The red and black lines in all panels, respectively, show $0.3f_{ce}$ and $0.1f_{ce}$.

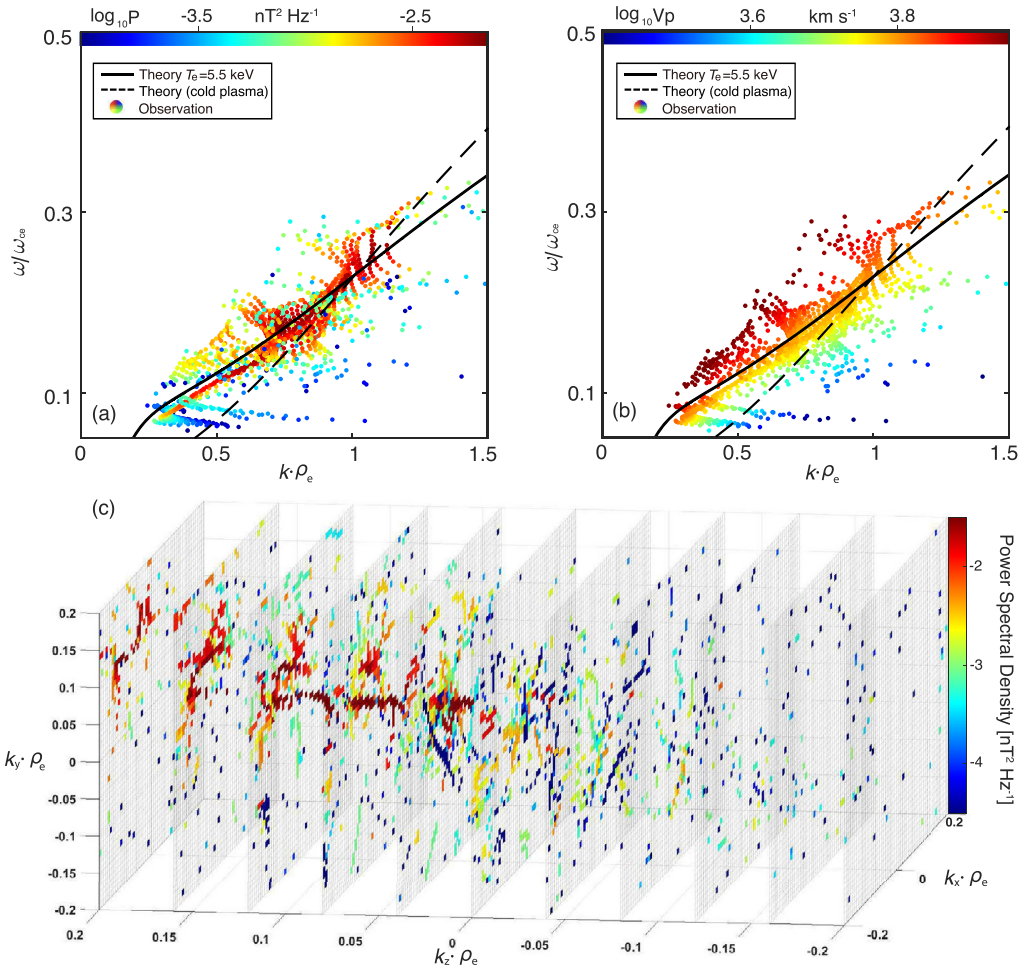


FIG. 4. Experimental determination of dispersion relation for whistler waves. (a) The dispersion relation with points colored by the wave power. (b) The dispersion relation with points colored by the wave phase velocity. (c) 3D \mathbf{K} -spectrum of the wave sliced from the k_z direction, with color denoting the accumulation of wave power continuously reconstructed by the DRAFT technique from 03:57:44.5–03:57:46 UT. Note that the black dashed line shows the dispersion relation for parallel whistler waves [24], and the black solid line shows the theory of whistler wave dispersion relation with $T_e = 5.5$ keV, $T_{e\perp}/T_{e\parallel} = 1.2$, $N_e = 0.15$ cm $^{-3}$, and $B_0 = 5$ nT.

process; at the same time, the experiment data points determined by DRAFT at $0.1\text{--}0.3 \omega_{ce}$ follow the same trend and are clustered around the theoretical curve of whistler wave dispersion relations. Now, considering the good agreement between the experimental dispersion relation and kinetic theory in Figs. 4(a) and 4(b), and the wave propagation dynamics in Fig. 3, we can confidently determine the fluctuations in Fig. 2 as whistler waves with phase and group velocity dispersion. In addition, we compare obtained wave characteristics with the cold plasma dispersion relation [24] for parallel whistler waves [see the black dashed lines in Figs. 4(a) and 4(b)]. As can be seen, for the same frequency, whistler waves in superhot plasmas generally have smaller wave numbers, faster phase velocities, and slower group velocities than whistler waves in cold plasmas. Moreover, the wave refractive index ($N = kc/\omega \sim 30$) derived from observations is well consistent with that predicted by hot plasma theory [69] ($N_{\text{hot}} \sim 20$), and is much smaller than that predicted by cold plasma theory [24] ($N_{\text{cold}} \sim 70$).

Certainly, we also can reorganize the data in Figs. 3(a)–3(d) in a different format, i.e., showing the dispersion relations P

(f , \mathbf{k}) [Fig. 4(a)] as functions of k_x , k_y , k_z to obtain the three-dimensional \mathbf{K} -spectrum of these whistler waves. Such a type of data reorganization is shown in Fig. 4(c), as an estimation of magnetic field energy distribution in the wave-vector space. As can be seen, the wave power is highest around the positive Z -direction and lowest around the negative Z -direction. Thus, we can estimate that the waves are primarily along the positive Z -direction, which is consistent with the background magnetic field [Fig. 1(c)] and indicated that the wave energy is guided approximately along the magnetic field. Such a 3D \mathbf{K} -spectrum could help us study the energy distribution of cross-scale wave-particle interactions and turbulence structure [70].

IV. WAVE GENERATION MECHANISM

Then we focus on the discussion about the excitation of these whistler waves. It is widely reported that, inside the dipolarizing flux bundles behind the reconnection fronts, electrons are preferentially heated in the directions perpendicular to the magnetic field by the betatron mechanism, leading to

high electron temperature and strong perpendicular temperature anisotropy therein [71–74]. Such electron temperature anisotropy is physically unstable and theoretically can produce a whistler mode branch [42,75]. Using WHAMP, we calculate the wave growth rate under the electron temperature anisotropy condition $T_{e\perp}/T_{e\parallel} \sim 1.2$ and find a positive wave growth rate at the frequency $\omega \sim 0.1\text{--}0.2\omega_{ce}$. The maximum growth rate $\gamma/\omega_{ce} \sim 0.05$ occurs at $\omega/\omega_{ce} = 0.14$, which is consistent with the observations. Interestingly, such perpendicular temperature anisotropy still holds inside the magnetic hole where the magnetic field magnitude dramatically drops, but right behind the magnetic hole, it clearly abates [Fig. 1(e)]. To further verify the wave generation mechanisms, we estimate the resonant energy during the propagation of these whistler waves. Based on the quasilinear cyclotron resonance condition [76], the electron resonance velocity is estimated as $v_{\parallel\text{res}} = (f - f_{ce})\lambda_{\parallel} = 5.8 \times 10^4$ km/s, or equivalently 9.7 keV. The electron distribution shows a transverse anisotropy (field-aligned flux much weaker than transverse flux, not shown here) for this resonant energy range, suggesting that the resonance energy estimated from wave measurements corresponds well with the anisotropic electron population from plasma measurements. Therefore, we conclude that these whistler waves are locally generated by the electron temperature anisotropy inside the magnetic hole.

V. CONCLUSIONS

In this Letter, we observed a whistler radio wave in a high-temperature magnetotail and constructed an experiment to determine its dispersion relation and 3D \mathbf{K} -spectrum by the MMS mission. Although some previous studies have focused on the propagation properties of whistlers in the solar wind and magnetopause (low-temperature areas), we believe this is the first determination of the dispersion relation for whistler waves in superhot ($T_e > 5$ keV) plasmas. Our experimental results align well with kinetic theory, by which we gain direct insight into the intricate interplay between whistler frequency and group velocity. We also find that these whistler waves are locally generated by the electron temperature anisotropy developed inside the magnetic hole. These findings unveil the nature of whistler waves and can be helpful in controlled radio excitation and transport, particularly within mediums of superhot plasmas in the laboratory and space.

ACKNOWLEDGMENTS

We thank the MMS Data Center [77] for providing the data. This work was supported by NSFC Grants No. 42125403, No. 41821003, and “the Fundamental Research Funds for the Central Universities.”

-
- [1] R. L. Stenzel, Whistler waves in space and laboratory plasmas, *J. Geophys. Res.* **104**, 14379 (1999).
 - [2] C.-Y. Tu and E. Marsch, MHD structures, waves and turbulence in the solar wind: Observations and theories, *Space Sci. Rev.* **73**, 1 (1995).
 - [3] W. H. Preece, Earth currents, *Nature (London)* **49**, 554 (1894).
 - [4] H. Barkhausen, Two phenomena revealed with the help of new amplifiers, *Z. Phys.* **20**, 401 (1919).
 - [5] M. Gołkowski, N. C. Gross, R. C. Moore, B. R. T. Cotts, and M. Mitchell, Observation of local and conjugate ionospheric perturbations from individual oceanic lightning flashes, *Geophys. Res. Lett.* **41**, 273 (2014).
 - [6] R. A. Helliwell and M. G. Morgan, Atmospheric whistlers, *Proc. IRE.* **47**, 200 (1959).
 - [7] C. Cattell *et al.*, Discovery of very large amplitude whistler-mode waves in Earth’s radiation belts, *Geophys. Res. Lett.* **35**, L011105 (2008).
 - [8] D. Cao *et al.*, MMS observations of whistler waves in electron diffusion region, *Geophys. Res. Lett.* **44**, 3954 (2017).
 - [9] S. C. Teng, F. Y. Wu, Y. Harada, J. Bortnik, F. Zonca, L. Chen, and X. Tao, Whistler-mode chorus waves at Mars, *Nat. Commun.* **14**, 3142 (2023).
 - [10] C. T. Russell, T. L. Zhang, M. Delva, W. Magnes, R. J. Strangeway, and H. Y. Wei, Lightning on Venus inferred from whistler-mode waves in the ionosphere, *Nature (London)* **450**, 661 (2007).
 - [11] J. B. Cao, X. H. Wei, A. Y. Duan, H. S. Fu, T. L. Zhang, H. Reme, and I. Dandouras, Slow magnetosonic waves detected in reconnection diffusion region in the earth’s magnetotail, *J. Geophys. Res.* **118**, 1659 (2013).
 - [12] X. H. Wei, J. B. Cao, G. C. Zhou, O. Santolík, H. Rème, I. Dandouras, N. Cornilleau-Wehrlin, E. Lucek, C. M. Carr, and A. Fazakerley, Cluster observations of waves in the whistler frequency range associated with magnetic reconnection in the Earth’s magnetotail, *J. Geophys. Res.* **112**, A10225 (2007).
 - [13] G. P. Chernov, Whistlers in the solar corona and their relevance to fine structures of type IV radio emission, *Sol. Phys.* **130**, 75 (1990).
 - [14] Y. Tong, I. Y. Vasko, A. V. Artemyev, S. D. Bale, and F. S. Mozer, Statistical study of whistler waves in the solar wind at 1 Au, *Astrophys. J.* **878**, 41 (2019).
 - [15] G. T. Roberg-Clark, J. F. Drake, C. S. Reynolds, and M. Swisdak, Suppression of electron thermal conduction in the high β intracluster medium of galaxy clusters, *Astrophys. J. Lett.* **830**, L9 (2016).
 - [16] C. S. Ng, A. Bhattacharjee, K. Germaschewski, and S. Galtier, Anisotropic fluid turbulence in the interstellar medium and solar wind, *Phys. Plasmas.* **10**, 1954 (2003).
 - [17] P. Zhu and R. W. Boswell, Ar I laser generated by Landau damping of whistler waves at the lower hybrid frequency, *Phys. Rev. Lett.* **63**, 2805 (1989).
 - [18] D. A. Spong *et al.*, First direct observation of runaway-electron-driven whistler waves in tokamaks, *Phys. Rev. Lett.* **120**, 155002 (2018).
 - [19] R. L. Stenzel, Whistler waves with angular momentum in space and laboratory plasmas and their counterparts in free space, *Adv. Phys.* **X 1**, 687 (2016).
 - [20] Y. Zhang, H. Matsumoto, and H. Kojima, Bursts of whistler mode waves in the upstream of the bow shock: Geotail observations, *J. Geophys. Res.* **103**, 20529 (1998).

- [21] X. Li and S. R. Habbal, Electron kinetic firehose instability, *J. Geophys. Res.* **105**, 27377 (2000).
- [22] S. P. Gary, *Theory of Space Plasma Microinstabilities* (Cambridge University Press, Cambridge, England, 1993).
- [23] W. Li *et al.*, Global distribution of whistler-mode chorus waves observed on the Themis spacecraft, *Geophys. Res. Lett.* **36**, L09104 (2009).
- [24] T. H. Stix, *Waves in Plasmas* (Springer Science & Business Media, New York, 1992).
- [25] H. S. Fu *et al.*, ULF waves associated with solar wind deceleration in the Earth's foreshock, *Chin. Phys. Lett.* **26**, 119402 (2009).
- [26] M. J. Houghton, Hot plasma theory of whistler mode wave packet propagation along a non-uniform magnetic field, *Plasma Phys.* **3**, 611 (1969).
- [27] H. S. Fu *et al.*, Whistler-mode waves inside flux pileup region: Structured or unstructured? *J. Geophys. Res.* **119**, 9089 (2014).
- [28] X. H. Deng and H. Matsumoto, Rapid magnetic reconnection in the earth's magnetosphere mediated by whistler waves, *Nature (London)*. **410**, 557 (2001).
- [29] D. Biskamp, E. Schwarz, and J. F. Drake, Two-dimensional electron magnetohydro-dynamic turbulence, *Phys. Rev. Lett.* **76**, 1264 (1996).
- [30] S. Galtier and A. Bhattacharjee, Anisotropic weak whistler wave turbulence in electron magnetohydrodynamics, *Phys. Plasmas*. **10**, 3065 (2003).
- [31] C. Liu, E. Hirvijoki, G.-Y. Fu, D. P. Brennan, A. Bhattacharjee, and C. Paz-Soldan, Role of kinetic instability in runaway-electron avalanches and elevated critical electric fields, *Phys. Rev. Lett.* **120**, 265001 (2018).
- [32] N. S. Artekha and D. R. Shklyar, Kinetic description of a whistler wave propagating in plasma along the magnetic field, *Plasma Phys. Rep.* **48**, 754 (2022).
- [33] A. V. Artemyev, O. Agapitov, D. Mourenas, V. Krasnoselskikh, V. Shastun, and F. Mozer, Oblique whistler-mode waves in the Earth's inner magnetosphere: Energy distribution, origins, and role in radiation belt dynamics, *Space Sci. Rev.* **200**, 261 (2016).
- [34] A. V. Artemyev, O. V. Agapitov, D. Mourenas, V. V. Krasnoselskikh, and F. S. Mozer, Wave energy budget analysis in the Earth's radiation belts uncovers a missing energy, *Nat. Commun.* **6**, 1 (2015).
- [35] M. Oka *et al.*, Electron scattering by high-frequency whistler waves at Earth's bow shock, *Astrophys. J. Lett.* **842**, L11 (2017).
- [36] C. Lacombe, O. Alexandrova, L. Matteini, O. Santolík, N. Cornilleau-Wehrin, A. Mangeney, Y. de Conchy, and M. Maksimovic, Whistler mode waves and the electron heat flux in the solar wind: *Cluster* observations, *Astrophys. J.* **796**, 5 (2014).
- [37] H. S. Fu, Y. Xu, A. Vaivads, and Y. V. Khotyaintsev, Super-efficient electron acceleration by an isolated magnetic reconnection, *Astrophys. J. Lett.* **870**, L22 (2019).
- [38] J. D. Strachan *et al.*, High-temperature plasmas in a tokamak fusion test reactor, *Phys. Rev. Lett.* **58**, 1004 (1987).
- [39] Q. Ma *et al.*, Very oblique whistler mode propagation in the radiation belts: Effects of hot plasma and Landau damping, *Geophys. Res. Lett.* **44**, 05712 (2017).
- [40] W. Baumjohann and R. Nakamura, Magnetospheric contributions to the terrestrial magnetic field, *Geomagnetism*. **5**, 77 (2007).
- [41] Y. Yu, H. S. Fu, and Z. Wang, Dipolarization fronts in cold-dense and hot-tenuous plasma sheet conditions: A comparative study, *J. Geophys. Res.* **128**, e2022JA031141 (2023).
- [42] D. Stansby, T. S. Horbury, C. H. K. Chen, and L. Matteini, Experimental determination of whistler wave dispersion relation in the solar wind, *Astrophys. J. Lett.* **829**, L16 (2016).
- [43] Z. H. Zhong *et al.*, Evidence for whistler waves propagating into the electron diffusion region of collisionless magnetic reconnection, *Geophys. Res. Lett.* **49**, e2021GL097387 (2022).
- [44] D. B. Graham *et al.*, Whistler emission in the separatrix regions of asymmetric magnetic reconnection, *J. Geophys. Res.* **121**, 1934 (2016).
- [45] Y. Narita *et al.*, On electron-scale whistler turbulence in the solar wind, *Astrophys. J. Lett.* **827**, L8 (2016).
- [46] P. Lebrun, Cryogenics for the large hadron collider, *IEEE Trans. Appl. Supercond.* **10**, 1500 (2000).
- [47] M. Stix, *The Sun: An Introduction* (Springer Science & Business Media, Berlin, 2004).
- [48] W. Baumjohann and R. A. Treumann, *Basic Space Plasma Physics* (World Scientific, Singapore, 1996).
- [49] A. Y. Potekhin, D. A. Baiko, P. Haensel, and D. G. Yakovlev, Transport properties of degenerate electrons in neutron star envelopes and white dwarf cores, *Astron. Astrophys.* **346**, 345 (1999).
- [50] D. Page and S. Reddy, Forecasting Neutron star temperatures: Predictability and variability, *Phys. Rev. Lett.* **111**, 241102 (2013).
- [51] J. B. Cao *et al.*, Joint observations by cluster satellites of bursty bulk flows in the magnetotail, *J. Geophys. Res.* **111**, A04206 (2006).
- [52] H. S. Fu, Y. V. Khotyaintsev, A. Vaivads, A. Retinò, and M. André, Energetic electron acceleration by unsteady magnetic reconnection, *Nat. Phys.* **9**, 426 (2013).
- [53] J. L. Burch, T. E. Moore, R. B. Torbert, and B. L. Giles, Magnetospheric multiscale overview and science objectives, *Space Sci. Rev.* **199**, 5 (2016).
- [54] W. Z. Zhang, H. S. Fu, J. B. Cao, Y. Y. Liu, J. S. Zhao, Z. Z. Guo, Z. Wang, and T. Y. Wang, DRAFT: A method for wave analyses in space plasmas, *Astrophys. J.* **936**, 176 (2022).
- [55] C. Pollock *et al.*, Fast plasma investigation for magnetospheric multiscale, *Space Sci. Rev.* **199**, 331 (2016).
- [56] R. B. Torbert *et al.*, The FIELDS instrument suite on MMS: Scientific objectives, measurements, and data products, *Space Sci. Rev.* **199**, 105 (2016).
- [57] H. S. Fu, E. E. Grigorenko, C. Gabrielse, C. M. Liu, S. Lu, K. J. Hwang, X. Z. Zhou, Z. Wang, and F. Chen, Magnetotail dipolarization fronts and particle acceleration: A review, *Sci. China Earth Sci.* **63**, 235 (2020).
- [58] H. S. Fu, Y. V. Khotyaintsev, A. Vaivads, M. André, and S. Y. Huang, Occurrence rate of earthward-propagating dipolarization fronts, *Geophys. Res. Lett.* **39**, L10101 (2012).
- [59] H. S. Fu, M. J. Zhao, Y. Yu, and Z. Wang, A new theory for energetic electron generation behind dipolarization front, *Geophys. Res. Lett.* **47**, e2019GL086790 (2020).
- [60] H. S. Fu *et al.*, Dipolarization fronts as a consequence of transient reconnection: In situ evidence, *Geophys. Res. Lett.* **40**, 6023 (2013).
- [61] H. S. Fu, Y. V. Khotyaintsev, A. Vaivads, M. André, and S. Y. Huang, Electric structure of dipolarization front at sub-proton scale, *Geophys. Res. Lett.* **39**, L06105 (2012).

- [62] M. J. Zhao, H. S. Fu, C. M. Liu, Z. Z. Chen, Y. Xu, B. L. Giles, and J. L. Burch, Energy range of electron rolling pin distribution behind dipolarization front, *Geophys. Res. Lett.* **46**, 2390 (2019).
- [63] Y. Xu, H. S. Fu, C. Norgren, S. Toledo-Redondo, C. M. Liu, and X. C. Dong, Ionospheric cold ions detected by mms behind dipolarization fronts, *Geophys. Res. Lett.* **46**, 7883 (2019).
- [64] Y. Yu, H. S. Fu, J. B. Cao, Y. Y. Liu, and Z. Wang, Electron rolling-pin distribution inside magnetic hole, *Astrophys. J.* **926**, 199 (2022).
- [65] Y. Yu, Z. Wang, H. S. Fu, and J. B. Cao, Direct evidence of interchange instabilities at dipolarization fronts, *J. Geophys. Res.* **127**, e2022JA030805 (2022).
- [66] O. Santolík, M. Parrot, and F. Lefeuvre, Singular value decomposition methods for wave propagation analysis, *Radio Sci.* **38**, 10 (2003).
- [67] C. M. Liu, H. S. Fu, Y. Y. Liu, and Y. Xu, Kinetics of magnetic hole behind dipolarization front, *Geophys. Res. Lett.* **48**, e2021GL093174 (2021).
- [68] K. Rönmark, WHAMP—Waves in homogeneous, anisotropic, multicomponent plasmas, Kiruna Geofysiska Institute Technical Report **14**, 179 (1982).
- [69] S. Sazhin, *Whistler-Mode Waves in a Hot Plasma* (Cambridge University Press, Cambridge, 1993).
- [70] W. Z. Zhang, H. S. Fu, J. B. Cao, Z. Wang, and Y. Y. Liu, Properties of the turbulence and topology in a turbulent magnetic reconnection, *Astrophys. J.* **953**, 23 (2023).
- [71] H. S. Fu, Y. V. Khotyaintsev, M. André, and A. Vaivads, Fermi and betatron acceleration of suprathermal electrons behind dipolarization fronts, *Geophys. Res. Lett.* **38**, L16104 (2011).
- [72] Yu. V. Khotyaintsev, C. M. Cully, A. Vaivads, M. André, and C. J. Owen, Plasma jet braking: Energy dissipation and nonadiabatic electrons, *Phys. Rev. Lett.* **106**, 165001 (2011).
- [73] H. S. Fu, A. Vaivads, Y. V. Khotyaintsev, M. André, J. B. Cao, V. Olshevsky, J. P. Eastwood, and A. Retinò, Intermittent energy dissipation by turbulent reconnection, *Geophys. Res. Lett.* **44**, 37 (2017).
- [74] W. D. Fu, H. S. Fu, J. B. Cao, Y. Yu, Z. Z. Chen, and Y. Xu, Formation of rolling-pin distribution of suprathermal electrons behind dipolarization fronts, *J. Geophys. Res.* **127**, e2021JA029642 (2022).
- [75] J. S. Zhao, Properties of whistler waves in warm electron plasmas, *Astrophys. J.* **850**, 13 (2017).
- [76] C. F. Kennel and H. E. Petschek, Limit on stably trapped particle fluxes, *J. Geophys. Res.* **71**, 1 (1966).
- [77] <https://lasp.colorado.edu/mms/sdc/public/>.